JACS
JOURNAL OF THE AMERICAN CHEMICAL SOCIETY

Article

pubs.acs.org/JACS

Effects of the Protein Environment on the Spectral Properties of Tryptophan Radicals in *Pseudomonas aeruginosa* Azurin

Caterina Bernini,[†] Tadeusz Andruniów,[‡] Massimo Olivucci,[†,§] Rebecca Pogni,[†] Riccardo Basosi,[†] and Adalgisa Sinicropi*[,†]

[†]Dipartimento di Biotecnologie, Chimica e Farmacia, Università di Siena, Via A. Moro 2, 53100 Siena, Italy

[‡]Quantum Chemistry and Molecular Modelling Lab, Institute of Physical and Theoretical Chemistry, Wroclaw University of Technology, Wyb. Wyspianskiego 27, 50-370 Wroclaw, Poland

[§]Chemistry Department, Bowling Green State University, Bowling Green, Ohio 43403, United States

Supporting Information

ABSTRACT: Many biological electron-transfer reactions involve short-lived tryptophan radicals as key reactive intermediates. While these species are difficult to investigate, the recent photogeneration of a long-lived neutral tryptophan radical in two *Pseudomonas aeruginosa* azurin mutants (Az48W and ReAz108W) made it possible to characterize the electronic, vibrational, and magnetic properties of such species and their sensitivity to the molecular environment. Indeed, in Az48W the radical is embedded in the hydrophobic core while, in ReAz108W it is solvent-exposed. Here we use density functional theory and multiconfigurational perturbation theory to construct quantum-mechanics/molecular-mechanics models of Az48W$^{\bullet}$ and ReAz108W$^{\bullet}$ capable of reproducing specific features of their observed UV−vis, resonance Raman, and electron paramagnetic resonance spectra. The results show that the models can correctly replicate the spectral changes imposed by the two contrasting hydrophobic and hydrophilic environments. Most importantly, the same models can be employed to disentangle the molecular-level interactions responsible for such changes. It is found that the control of the hydrogen bonding between the tryptophan radical and a single specific surface water molecule in ReAz108W$^{\bullet}$ represents an effective means of spectral modulation. Similarly, a specific electrostatic interaction between the radical moiety and a Val residue is found to control the Az48W$^{\bullet}$ excitation energy. These modulations appear to be mediated by the increase in nitrogen negative charge (and consequent increase in hydrogen bonding) of the spectroscopic D_2 state with respect to the D_0 state of the chromophore. Finally, the same protein models are used to predict the relaxed Az48W$^{\bullet}$ and ReAz108W$^{\bullet}$ D_2 structures, showing that the effect of the environment on the corresponding fluorescence maxima must parallel that of D_0 absorption spectra.

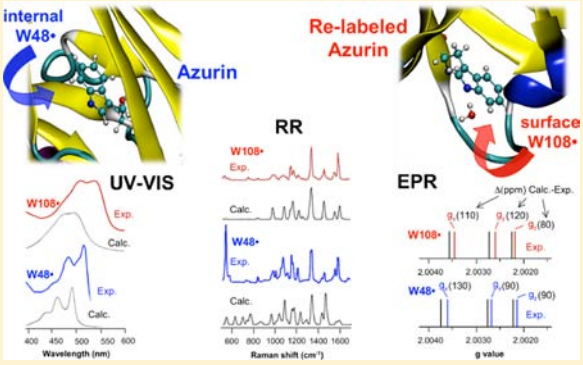

1. INTRODUCTION

Redox-active tryptophan radicals are key intermediates in many enzymatic reactions.[1−3] For instance, they play a role in DNA photolyase,[2,4,5] cytochrome *c* peroxidase,[6−8] ribonucleotide reductase mutants,[9−11] lignin peroxidase,[12] and versatile peroxidase.[13−17]

Tryptophan radicals are generated either by electron transfer (ET) to an acceptor oxidant or via a net H-atom transfer (HAT). The first process (generally occurring over long distances) leads to the formation of a cationic radical (TrpH$^{\bullet+}$) which is followed, in most cases, by proton release to generate a neutral radical (Trp$^{\bullet}$). The second process yields Trp$^{\bullet}$ through a simultaneous transfer of electrons and protons.[1,3,18,19]

The demonstrated occurrence of Trp radicals in biological ET stimulated a number of experimental and theoretical investigations of these intermediates. From the experimental point of view, techniques of choice for the detection and identification of Trp radicals are magnetic spectroscopies, such as electron paramagnetic resonance (EPR) and electron−nuclear double-resonance (ENDOR) spectroscopy.[13,14,20−22]

Theoretical studies on Trp or indole radical model systems have been reported both *in vacuo*[23−26] and in condensed phases.[27] They were based on density functional theory (DFT) calculations and, in combination with the experimental EPR data, were mainly intended to elucidate the nature (neutral deprotonated or cationic protonated) of the radicals.

In recent studies[28,29] we focused on the computational characterization of Trp radicals within protein matrices in which such transient species have a catalytic role. In particular, we have shown that quantum-mechanics/molecular-mechanics (QM/MM) computations, based on a DFT/CHARMM protocol, allow for the accurate simulation of the EPR spectral parameters of a Trp radical in *Pleurotus eryngii* versatile

Received: January 15, 2013
Published: March 4, 2013

   dx.doi.org/10.1021/ja400464n | *J. Am. Chem. Soc.* 2013, 135, 4822−4833

peroxidase (VP), in lignin peroxidase (LiP) and its E250Q +E168Q variant, and in a *Coprinus cinereus* peroxidase triple variant (D178W+R257E+R271D). Indeed, the fit between computed and measured **g**-tensors, hyperfine coupling constants (hfcc's), and Mulliken spin densities allowed for the unambiguous assignment of the experimentally detected Trp radical to a neutral or cationic species. Furthermore, the employed QM/MM protocol provided additional details on the environment surrounding the radical and on the role played by the nearby protein residues and solvent water molecules in affecting the electronic and geometrical structure of the radical intermediate.

The possibility to characterize, beyond the EPR analysis, the electronic and vibrational properties of Trp radicals opens the alley to complementary information on these important reactive intermediates and to a comprehensive understanding of Trp-mediated ET reactions. Despite this, optical and vibrational spectroscopies, especially resonance Raman (RR) spectroscopies, have been rarely employed to study these species.[30,31]

The recent photogeneration of a *long-lived* Trp$^{\bullet}$ in two *Pseudomonas aeruginosa* azurin mutants, [Y72F/Y108F]AzCu-(II) (Az48W) and the rhenium-labeled Az108W mutant [Re(I)$(CO)_3$(4,7-dimethyl-1,10-phenanthroline)(Q107H)]-(W48F/Y72F/H83Q/Y108W)AzM(II) [M = Cu, Zn] (ReAz108W), provided the unique opportunity to obtain the electronic, magnetic, and vibrational spectra of these radical species[21,22,32] and identify the spectral signatures of Trp radicals that are sensitive to the local environment. Indeed, in Az48W the radical (W48$^{\bullet}$) is buried in the hydrophobic core (see Figure 1, left), while it is solvent-exposed (W108$^{\bullet}$) in ReAz108W (see Figure 1, right).

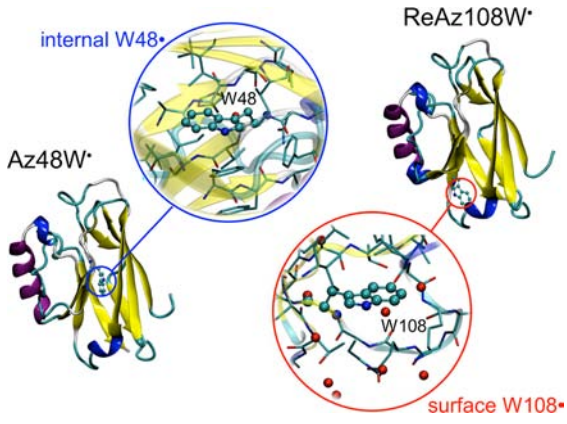

Figure 1. Structural view of *Pseudomonas aeruginosa* azurin [Y72F/Y108F]AzCu(II) (Az48W$^{\bullet}$) (left) and [Re(I)$(CO)_3$(4,7-dimethyl-1,10-phenanthroline)(Q107H)](W48F/Y72F/H83Q/Y108W)AzM-(II) [M = Cu, Zn] (ReAz108W$^{\bullet}$) (right) mutants. The positions of the internal W48$^{\bullet}$ and surface W108$^{\bullet}$ residues are highlighted.

In the following, we employ different QM/MM protocols to compute the absorption maxima (λ_{max}), the vibrationally resolved UV−vis spectra, the RR spectra, and EPR spectral parameters (**g**-tensors and hfcc's) of W48$^{\bullet}$ and W108$^{\bullet}$. To the best of our knowledge, this is the first QM/MM study devoted to the characterization of Trp radicals inside the matrix of blue copper proteins. As we will point out below, this is also the first time that a QM/MM model is constructed using geometry optimizations carried out at the computationally demanding CASPT2 level of theory. The results show that the computed spectral data compare well with the experimental values. Remarkably, we have been able to confirm the nature of the Trp radical as neutral, H-bonded in ReAz108W$^{\bullet}$ and not H-bonded in Az48W$^{\bullet}$, and reproduce specific features of the EPR, UV−vis, and RR spectra. In particular, we have computed with a high level of accuracy the **g**-tensor anisotropy of Trp$^{\bullet}$, obtained with an unprecedented resolution using a 700 GHz EPR instrument,[22] and elucidated the origin of the double-band line shape of the UV−vis spectrum. We have also been able to reproduce the observed spectral shifts of Trp$^{\bullet}$ embedded in contrasting hydrophobic and hydrophilic environments and identify the molecular-level interactions responsible for such spectral changes. The QM/MM models have also been employed to predict the excited-state equilibrium geometries and corresponding emission maxima.

2. MODELS AND METHODS

Protein Setup. Initial structures for ReAz108W (PDB code: 1R1C; resolution 1.90 Å) and Az48W (PDB code: 4AZU; resolution 1.90 Å) were obtained from the Protein Data Bank. Results of PROPKA2.0[33] runs were used, in combination with visual inspection, to assign the protonation states of all titratable residues (aspartic acid, glutamic acid, and histidine) at the experimental pH of 7.2. Missing hydrogen atoms were added by the psfgen module of VMD, version 1.8.7.[34] The protonated systems, with crystallographic water molecules, were neutralized with sodium and chlorine ions (0.15 M ionic strength) and fully solvated in rectangular boxes (59 × 58 × 62 Å^3 for ReAz108W$^{\bullet}$ and 63 × 54 × 59 Å^3 for Az48W$^{\bullet}$) of TIP3P water molecules[35] using the autoionize and solvate modules of VMD. Solvent boxes were created with a layer of at least 10 Å of water molecules around each protein atom and included 5880 and 5410 water molecules for ReAz108W and Az48W, respectively.

Preparatory Force Field Calculations. AMBER force field[36−38] and TIP3P water model[35] were used for both pure MM and hybrid QM/MM calculations. All available force field parameters and charges were taken from the parm99.dat library.[37] For the treatment of the Cu(I) active site in the Az48W$^{\bullet}$ radical model, previous published parameters[39,40] were used, and partial atomic charges were determined with the Gaussian03 software package[41] using a restrained electrostatic potential (RESP) procedure[37] (see Table S1 in the Supporting Information (SI)). For the ReAz108W$^{\bullet}$ radical model, the copper was replaced by Zn(II) since the experiments were carried out on both the Cu(II) ReAz108W$^{\bullet}$ radical and the Zn(II)-substituted protein and showed that the spectra are independent of the metal center (Cu(II) or Zn(II)), indicating that the electronic coupling between the radical and Cu(II) is negligible (Cu−Cγ (W108) distance is 16.7 Å). RESP partial atomic charges were calculated also for the Re(I)$(CO)_3$(1,10-phenanthroline)(H107) complex and for the Trp N1-deprotonated radical (see Table S2). The solvated systems were relaxed by performing classical energy minimization and molecular dynamics (MD) simulations with the NAMD 2.7 code.[42] The positions of the hydrogen atoms and solvent water molecules were first energy minimized and equilibrated at 298 K and 1 atm for 1 ns with a time step of 1 fs. Electrostatic interactions were taken into account using the Particle Mesh Ewald (PME) method,[43] and Periodic Boundary Conditions (PBC) were applied. A further 10-ns equilibration was then carried out in which even the protein side chains were left free to equilibrate. During the MD simulations the coordinates of non-hydrogen atoms of the Cu/Zn active site, Re(I)$(CO)_3$(1,10-phenanthroline)(H107) complex, and protein backbone atoms were kept fixed to the crystal structure. A snapshot was taken at the end of the MD equilibration runs of both systems. The extracted snapshots were energy minimized and used as starting structures for the following QM/MM computations.

QM/MM Calculations. All QM/MM calculations were performed with the MOLCAS 7.4 package,[44] coupled with a modified version of the MM package Tinker 4.2.[45] as originally described in refs 46 and 47.

dx.doi.org/10.1021/ja400464n | J. Am. Chem. Soc. 2013, 135, 4822−4833

An electronic embedding (EE) scheme was applied, using hydrogen link atoms (HLA) with a scaled-charge model[48−50] to treat the QM/MM boundary region (see the SI for further details). The frontier is placed at the CO−CαH bonds of H107 in ReAz108W$^\bullet$ and N47 in Az48W$^\bullet$, and at the NH−CαH bonds of M109 in ReAz108W$^\bullet$ and V49 in Az48W$^\bullet$ (see Scheme 1). The QM model employed in QM/MM calculations for both systems includes the Trp residue, H1-deprotonated. In the case of ReAz108W$^\bullet$ the QM model includes also the solvent water molecule forming a hydrogen bond with the pyrrolic nitrogen. QM/MM geometry optimizations were performed using (i) the unrestricted open-shell DFT with the B3LYP functional, (ii) the complete active space self-consistent field (CASSCF), and (iii) the multireference perturbation theory method (CASPT2)[51] for the QM part. The AMBER force field[36−38] was employed for the treatment of the MM part. The selected CASSCF active space comprises the full π-system and the nitrogen lone pair (11 electrons in 10 orbitals). A mixed basis set (hereafter called 6-31G**#) was used: the 6-31G** basis set for all atoms except pyrrolic nitrogen and the water molecule involved in the formation of hydrogen bond with Trp$^\bullet$, for which the 6-31++G** basis set was used. Morokuma's scheme as implemented in MOLCAS 7.4[44] was applied to constrain the LA position on the line connecting the QM and the MM atoms.

Scheme 1. QM Region Employed in QM/MM Calculations for ReAz108W$^\bullet$ [a] and Az48W$^\bullet$

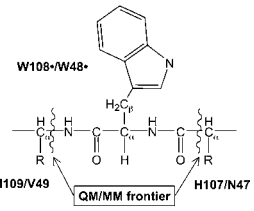

[a]A water molecule hydrogen bonded to the pyrrolic nitrogen is also included in ReAz108W$^\bullet$.

EPR, UV−Vis, and RR Computations. EPR magnetic parameters have been computed via single-point calculations on the B3LYP/AMBER optimized structures using the ORCA2.8 program package[52] with an EE scheme, in which fixed MM point charges are included in the one-electron QM Hamiltonian and the QM/MM electrostatic interactions are evaluated from the QM electrostatic potential and the MM charges. The B3LYP[53−55] and PBE0[56] functionals were used in combination with the polarized triple-ζ valence basis set TZVP or the Barone's EPR-II basis set.[57−59] Vertical transition energies and oscillator strengths for the singlet excited states of Trp$^\bullet$ were obtained from CASPT2/ANO-S-VDZP calculations on CASPT2/AMBER, CASSCF/AMBER, and B3LYP/AMBER optimized geometries. Excitation energies were also computed from time-dependent DFT (TD-DFT) calculations with Gaussian09[60] using B3LYP[53−55] and PBE0[56] functionals in combination with the 6-31+G*, TZVP, and aug-cc-pVDZ basis sets. The UV−vis absorption spectra were analyzed in the framework of the independent mode displaced harmonic oscillator (IMDHO) model using the "orca_asa" module[61] implemented in ORCA2.8[52] for the calculation of optical bandshapes. The spectra were simulated using a homogeneous line width of 700 cm^{-1} (for ReAz108W$^\bullet$) or 200 cm^{-1} (for Az48W$^\bullet$) and the CASPT2 vertical excitation energies. Vibrational frequencies and gradient calculations used for both UV−vis and RR spectra simulations have been carried out with ORCA2.8 at the B3LYP/TZVP level of theory.

Resonance Raman spectra for both radicals were calculated for 514.5 nm excitation wavelength, which is in agreement with the lower energy absorption band for Az48W$^\bullet$ and approaches the higher energy absorption band for ReAz108W$^\bullet$. Ground-state normal modes and excited-state gradient at the ground-state equilibrium structure in the absence of normal-mode rotation (Duschinsky rotation) and vibrational frequency change upon electronic excitation were used to simulate the spectra.[62] The RR intensity calculation is based on time-dependent Heller's approximation assuming the IMDHO model.[61] Fundamental RR bands were only considered since the inclusion of overtones and combination bands did not introduce any significant changes in the intensity distribution within the 500−1700 cm^{-1} spectral range. Spectra were generated using a Gaussian broadening with a half-width of 20 cm^{-1}, while adiabatic transition energy, homogeneous broadening, and transition dipole moment were the same as in the absorption spectra simulation. The computed B3LYP-based Raman shifts were scaled down by 0.9816 to match the location of the most intense W7$^\bullet$ peak in the experimental spectra.

3. RESULTS AND DISCUSSION

3.1. EPR. The combined use of EPR/ENDOR spectroscopies and DFT-based QM/MM calculations turns out to be valuable for getting insight into the geometric and electronic structures of biologically important radical species as well as assigning them to a specific site in a protein.[28,29,63−68] In addition, it makes it possible to identify the main interactions (such as hydrogen bonding) inside the protein matrix that influence the magnetic spectroscopic parameters.

Here, we use a DFT/MM strategy to compute the magnetic properties (hfcc's, **g**-tensors, and Mulliken spin densities) of the solvent-exposed W108$^\bullet$ in ReAz108W$^\bullet$ and those of W48$^\bullet$ in the hydrophobic pocket of Az48W$^\bullet$. The EPR spectral features that characterize and differentiate the two radicals in the two different environments have been identified.

EPR spectra of Trp radicals usually exhibit an almost symmetrical four-line pattern dominated by the two β-methylene protons' hfcc's, $A(\beta\text{-H1})$ and $A(\beta\text{-H2})$. It is accepted that these values depend on the overlap with the spin density on C3 (see Scheme 2 for Trp numbering).[26,27]

Scheme 2. Numbering Scheme and g-Tensor Principal Axes Orientation of Trp$^\bullet$ with Respect to the Molecular Frame[a]

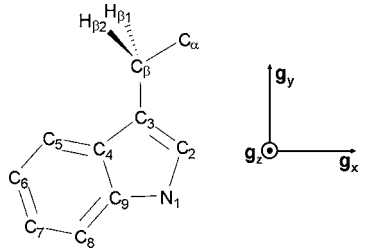

[a]g_x is in the pyrrole ring, almost parallel to the C9−N1 bond, g_z perpendicular to the ring plane, and g_y mutually perpendicular to the other two components.

The extent of this overlap and hence the hfcc values are a function of the rotation angle of the indole ring, ϕ, defined by the Cα−Cβ−C3−C2 dihedral angle, with respect to the protein backbone. For ϕ = 90° the two β-methylene protons are symmetrical with respect to the axis perpendicular to the indole ring and share the same amount of C3 spin density. Thus, their hfcc values are expected to be the same. The greater is the deviation in the value of ϕ from 90°, the larger is the difference between $A(\beta\text{-H1})$ and $A(\beta\text{-H2})$ values.

Our models computed at the B3LYP/AMBER level of theory, in which the Trp$^\bullet$ geometries are relaxed under the constraint imposed by the surrounding protein environment, show ϕ = −76.58° and 88.99° for ReAz108W$^\bullet$ and Az48W$^\bullet$, respectively. Both dihedral angles are in accord with those experimentally derived for ReAz108W$^\bullet$ (−76°) and Az48W$^\bullet$ (88°)[21] using the McConnell equation. On the other hand, the

Table 1. Experimental and Computed EPR g-Tensors (g_i) and hfcc Values (A_i in Gauss) for ReAz108W$^\bullet$ and Az48W$^\bullet$

	i	g_i	$A_i(\beta$-H1)	$A_i(\beta$-H2)	A_i(H5)	A_i(H7)	A_i(N)	A_i(N--H−OH)
				ReAz108W$^\bullet$				
expt[a]	x	2.00346	2.1	11.5	−6.0	≤|1|	≤1	−1.2
	y	2.00264	1.5	14.3	−2.1	−7.9	≤1	1.9
	z	2.00216	2.3	11.9	−4.8	−4.2	10.4	−0.8
	iso	2.00275	2.0	12.6	−4.3	−(4.0−4.4)	3.5−4.1	∼0.0
B3LYP/EPR-II	x	2.00357	1.6	12.0	−7.8	−1.6	−0.6	−0.7
	y	2.00276	1.3	14.9	−2.3	−7.4	−0.7	1.6
	z	2.00224	3.9	12.3	−5.9	−5.0	10.5	−0.6
	iso	2.00286	2.3	13.1	−5.3	−4.7	3.1	0.1
				Az48W$^\bullet$				
expt[a]	x	2.00361	6.6	9.0	−7.1	−1.8	≤1	NA
	y	2.00270	7.3	8.7	−1.8	−3.9	≤1	NA
	z	2.00215	5.0	7.4	−2.9	−4.9	11.8	NA
	iso	2.00282	6.3	8.4	−3.9	−3.5	3.9−4.6	NA
B3LYP/EPR-II	x	2.00374	5.7	10.7	−6.8	−1.3	−0.8	
	y	2.00279	8.5	7.7	−2.1	−4.3	−0.9	
	z	2.00224	6.1	7.9	−5.4	−6.4	11.5	
	iso	2.00292	6.8	8.8	−4.8	−4.0	3.3	

[a]Experimental **g**-tensors and hfcc's from refs 21. 22. For Trp numbering and **g**-tensor orientation see Scheme 2.

computed ϕ values of the optimized Trp$^\bullet$ are different from those derived from the X-ray structures (−81.87° and 89.83° for ReAz108W and Az48W, respectively). Thus, as reported also in a previous work,[28] the orientation of the oxidized residue diverges from the orientation in its reduced state. This finding suggests that the use of these ring rotation angles to discriminate between different radical sites within the crystallographic structure could lead to an erroneous assignment of the radical site. This might occur especially when these angles do not differ significantly.

The B3LYP/EPR-II computed hfcc values of Trp$^\bullet$ in ReAz108W$^\bullet$ and Az48W$^\bullet$ are gathered in Table 1 and are compared with experimental values from ref 21 (additional results obtained using the B3LYP/TZVP, PBE0/EPR-II, and PBE0/TZVP levels are reported in Table S4). For both systems, the computed hfcc's show a good agreement with those observed experimentally. In particular, the isotropic β-methylene protons' hfcc's, $A_{iso}(\beta$-H1) and $A_{iso}(\beta$-H2), are within ∼15% of the experimental data, which is well within the commonly accepted accuracy (∼10−20%) for hfcc calculation with DFT methods. These values are also consistent with the different computed ϕ values in the two systems. Indeed, the $A_{iso}(\beta$-H1) and $A_{iso}(\beta$-H2) for Az48W$^\bullet$ (6.8 and 8.8 G, respectively) differ by only 2 G, which is in accord with a structure having ϕ close to 90°. On the other hand, the same values computed for the Trp radical in ReAz108W$^\bullet$ are very different ($A_{iso}(\beta$-H1) = 2.3 G and $A_{iso}(\beta$-H2) = 13.1 G) and agree with a geometry featuring one of the two β-methylene protons much closer to the indole plane. This confirms the goodness of our models in reproducing the correct Trp$^\bullet$ orientation in the protein environment of ReAz108W$^\bullet$ and Az48W$^\bullet$. The accord between experimental and computed values is also satisfactory for the anisotropic hfcc's for the ring protons, A_i(H5) and A_i(H7), and the large anisotropic hfcc for N1, A_i(N1). As a consequence, there is also a good correlation (see Figure 2) between experimental and computed environmental, i.e., hydrophobic vs hydrophilic, shifts (Δ_{env}) in hfcc values (for each magnetically active nucleus reported in Table 1).

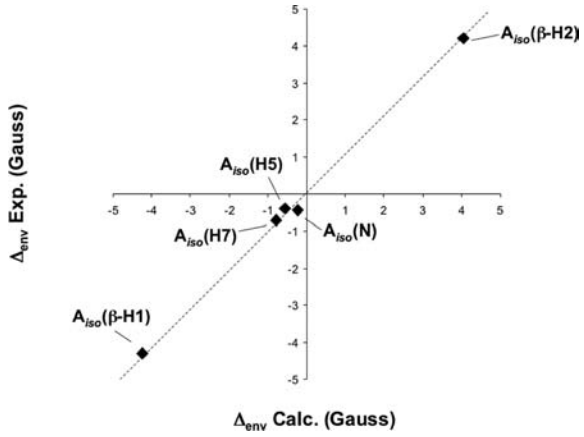

Figure 2. Correlation between experimental (Δ_{env} Exp.) and computed (Δ_{env} Calc.) environmental (hydrophobic vs hydrophilic) shifts in Trp$^\bullet$ EPR parameters $A_{iso}(\beta$-H1), $A_{iso}(\beta$-H2), A_{iso}(H5), A_{iso}(H7), and A_{iso}(N).

The EPR spectrum of Trp$^\bullet$ is also characterized by a small **g**-tensor anisotropy, which is a common feature of organic π-radicals with spin densities only on carbon or nitrogen atoms. Typical g-values are 2.0033−2.0036 for g_x, 2.0024−2.0027 for g_y, and 2.0022 for g_z. Experimentally, the small **g**-tensor anisotropy can be fully resolved only by using ultrahigh field and frequency EPR spectroscopy. Very recently, Stoll et al.[22] obtained a complete separation of the three principal **g**-tensor components of W108$^\bullet$ and W48$^\bullet$ using an EPR instrument at 700 GHz and 25 T.

The computed **g**-tensors for ReAz108W$^\bullet$ and Az48W$^\bullet$ are gathered in Table 1 and compared with those reported by Stoll et al.[22] In accord with the experimental values, the **g**-tensor anisotropy computed for W48$^\bullet$ is larger than that computed for W108$^\bullet$. In particular, a decrease in g_x value is computed going from W48$^\bullet$ to W108$^\bullet$. *This is consistent with our B3LYP/AMBER optimized models featuring a Trp$^\bullet$ not involved in hydrogen bonding at N1 in Az48W$^\bullet$ and a Trp$^\bullet$ H-bonded to a water molecule (with a N···H distance of ∼2.0 Å) in ReAz108W$^\bullet$.* Indeed, as pointed out in prior computational reports, the g_x

dx.doi.org/10.1021/ja400464n | J. Am. Chem. Soc. 2013, 135, 4822−4833

value can be used to discriminate if the indole nitrogen is near an H-donor.[26−29] We have shown that the g_x component of the radical is decreased when the length of the H-bond becomes shorter, i.e., the bond becomes stronger. This variation is also accompanied by a decrease of Mulliken spin density on C3 and N1 and an increase of the spin density on C2. This trend in π-spin densities variation is also reproduced, in this work, by the computed Mulliken spin densities of the buried Trp$^\bullet$ in Az48W$^\bullet$ in comparison to the solvent-exposed and H-bonded Trp$^\bullet$ in ReAz108W$^\bullet$ (see Table 2).

Table 2. McConnell-Derived π-Spin Densities and Computed Mulliken Spin Densities for ReAz108W$^\bullet$ and Az48W$^\bullet$

	ReAz108W$^\bullet$		Az48W$^\bullet$	
	expt[a]	B3LYP/EPR-II[b]	expt[a]	B3LYP/EPR-II[b]
N1	0.19	0.23	0.22	0.25
C2	NA	−0.03	NA	−0.08
C3	0.45	0.51	0.50	0.54
C4	NA	−0.10	NA	−0.10
C5	0.17	0.21	0.16	0.19
C6	NA	−0.07	NA	−0.05
C7	0.17	0.19	0.17	0.16
C8	NA	0.00	NA	0.00
C9	NA	0.06	NA	0.07
Cβ	NA	−0.03	NA	−0.03

[a]McConnell spin densities from experimental isotropic hfcc values.[21] Data reported for nitrogen reflect the average values within a plausible range of $A_i(N)$. [b]The total Mulliken spin density is equal to one adding the small contributions from the remaining QM atoms.

It is worth noting that the computed **g**-tensor values differ from the corresponding experimental values by at most 130 ppm, which is well within the accepted accuracy of 200 ppm (for organic radicals computed at the DFT level). *Such accuracy in reproducing the highly resolved experimental* ***g****-tensor values provides evidence of the quality of the QM/MM models and applied protocols and opens the way for its use as a predictive tool.*

3.2. UV−Vis. The difference absorption spectra of the photogenerated Trp$^\bullet$ exhibit a double-band pattern with relatively narrow peaks at 510 and 537 nm (2.43, 2.31 eV) for ReAz108W$^\bullet$ and at 486 and 516 nm (2.55, 2.41 eV) for Az48W$^\bullet$ (see red lines in Figure 3). This is in contrast to the single band observed in the spectrum for Trp$^\bullet$ in the gas phase (λ_{max} = 473 nm)[69] and in aqueous solution (λ_{max} = 510 nm).[70] Remarkably, the absorption spectra of the radical show a hypsochromic shift of ∼21−24 nm (0.10−0.12 eV) on going from the solvent-exposed environment of ReAz108W$^\bullet$ to the nonpolar environment of Az48W$^\bullet$. Thus, it is evident that, similarly to the EPR properties, the absorption spectra of the radical are sensitive to the local environment (hydrophobicity and/or hydrogen bonding).

In order to ensure the best possible accuracy in the simulation/prediction of the electronic spectra of ReAz108W$^\bullet$ and Az48W$^\bullet$, their ground- and excited-state (see section 3.4) equilibrium structures are determined at the *state-of-the-art* CASPT2 level of theory by using numerical gradients. Accordingly, in Table 3 we report the CASPT2/AMBER λ_{max}, excitation energies, oscillator strengths, and change in dipole moments for W108$^\bullet$ and W48$^\bullet$ computed on ground-state (D_0) CASPT2/AMBER (with a CAS(11,10) expansion in the reference CASSCF wave function) equilibrium geometries

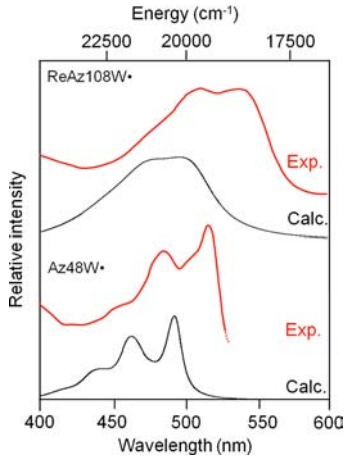

Figure 3. Experimental (red) and simulated (black) UV−vis spectra of ReAz108W$^\bullet$ (top) and Az48W$^\bullet$ (bottom). The experimental spectra are adapted from ref 21.

using the ANO-S-VDZP basis. The same values have also been computed on the CASSCF/AMBER and B3LYP/AMBER D_0 equilibrium geometries.

The excitation energies and oscillator strengths have also been evaluated at the TDDFT/AMBER level on the B3LYP/AMBER equilibrium geometries employing the B3LYP and PBE0 functionals together with the aug-cc-pVDZ basis set.

Both the CASPT2/AMBER and TDDFT/AMBER calculations indicate that the spectra of ReAz108W$^\bullet$ and Az48W$^\bullet$ arise from a single electronic transition which is characterized by an oscillator strength of 0.02−0.06. In fact, simulation of the vibrationally resolved electronic spectra in the 400−600 nm range (see Figure 3 and the Models and Methods section for details on the protocol we used to simulate the spectra) shows that the observed line shape of the visible absorption spectra of both W108$^\bullet$ and W48$^\bullet$ is correctly reproduced when taking into account its vibrational progression. The peaks at higher wavelengths with origin (0−0 adiabatic transition) computed at 19496 cm^{-1} (ReAz108W$^\bullet$) and at 20126 cm^{-1} (Az48W$^\bullet$), respectively, are governed by very active and low-frequency modes at 43, 69 cm^{-1} for ReAz108W$^\bullet$ and 69, 79 cm^{-1} for Az48W$^\bullet$ (see Figure 4).

The vibrational structure of the other blue-shifted peaks is induced by the modes with the largest values of Franck−Condon (FC) factors in the ranges of ∼1200−1600 cm^{-1} for ReAz108W$^\bullet$ and 1100−1500 cm^{-1} for Az48W$^\bullet$ (see Figure 4). See also the simulated spectra with a reduced line width shown in Figures S3 and S4 to appreciate the details of the computed vibronic structures.

The mode corresponding to the vertical excitation is the 1368 cm^{-1} mode in ReAz108W$^\bullet$ and the 1353 cm^{-1} mode in Az48W$^\bullet$ (see Figure 4). However, in each species there is also one additional mode (the 1351 cm^{-1} mode in ReAz10W$^\bullet$ and the 1367 cm^{-1} mode in Az48W$^\bullet$) of rather strong FC activity, which may contribute to the vertical excitation.

The CASPT2/AMBER vertical excitation energies of both radical species fall under the band at lower wavelengths and well reproduce the observed values with a blue-shift of 0.11−0.20 eV. We computed the CASPT2 excitations also without the empirical IPEA shift for the zero-order Hamiltonian. The resulting excitations are red-shifted by 0.18−0.20 eV in comparison with those computed with the corrected

dx.doi.org/10.1021/ja400464n | J. Am. Chem. Soc. 2013, 135, 4822−4833

Table 3. CASPT2/AMBER and TDDFT/AMBER Absorption Maxima λ_{max} (nm), Excitation Energies (eV), Oscillator Strengths (f_{osc}), and Change in Dipole Moments ($\Delta\mu$) for ReAz108W• and Az48W•

		ReAz108W•					Az48W•				
	SA[c]	state	λ_{max}	E_{exc}	f_{osc}	$\Delta\mu$	state	λ_{max}	E_{exc}	f_{osc}	$\Delta\mu$
CASPT2/ANO-S-VDZP//CASPT2(11,10)/6-31G**[#]											
CAS(11,10)[a]	5	3	480.2	2.59	0.0155	0.90	3	466.7	2.66	0.0128	1.81
CAS(11,10)[b]	5	3	517.2	2.40	0.0155	0.90	3	503.9	2.46	0.0128	1.81
CASPT2/ANO-S-VDZP//CASSCF(11,10)/6-31G**[#]											
CAS(11,10)[a]	5	3	471.6	2.63	0.0146	0.90	3	461.3	2.69	0.0125	1.79
CAS(11,10)[b]	5	3	508.0	2.44	0.0146	0.90	3	497.8	2.49	0.0125	1.79
CASPT2/ANO-S-VDZP//B3LYP/6-31G**[#]											
CAS(11,10)[a]	5	3	480.6	2.58	0.0162	1.07	3	466.0	2.66	0.0128	1.81
CAS(11,10)[b]	5	3	517.1	2.40	0.0162	1.07	3	502.9	2.47	0.0128	1.81
TD-B3LYP/aug-cc-pVDZ//B3LYP/6-31G**[#]		5	476.0	2.61	0.0558		3	465.6	2.66	0.0543	
TD-PBE0/aug-cc-pVDZ//B3LYP/6-31G**[#]		3	467.0	2.65	0.0457		3	451.7	2.74	0.0501	

[a]Computed using the standard IPEA Hamiltonian. [b]Computed without the IPEA shift. [c]State Average (SA) calculations on the lowest 5 states.

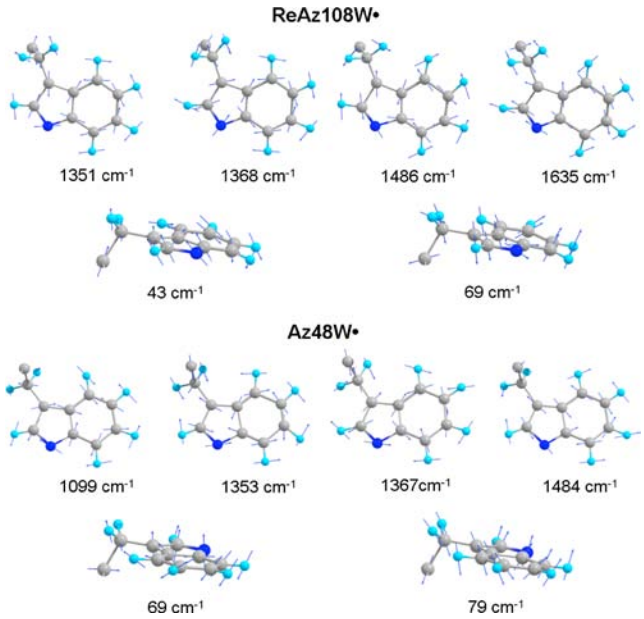

Figure 4. Normal modes with the largest values of Franck−Condon factors for W108• (top) and W48• (bottom).

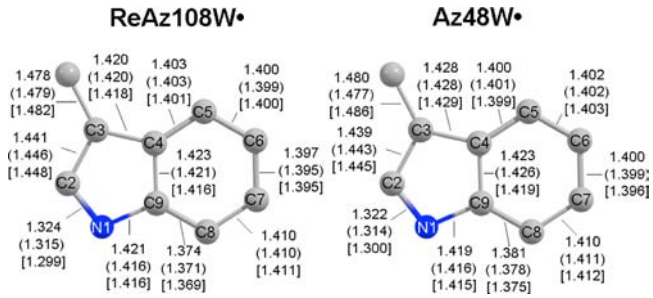

Figure 5. CASPT2/AMBER, B3LYP/AMBER (in parentheses), and CASSCF/AMBER optimized (in square brackets) geometries for W108• (left) and W48• (right). Bond lengths are given in Å.

Hamiltonian and display differences with the experimental values in the range of 0.01−0.09 eV.

Considering the CASPT2/AMBER values for the vertical excitation energies reported in Table 3, we compute a hypsochromic shift of 10−15 nm (0.05−0.08 eV) going from the solvent-exposed environment of ReAz108W• to the nonpolar environment of Az48W•, in agreement with the observed environmental shifts.

The small differences in the excitation energy among CASPT2/AMBER, CASPT2//CASSCF/AMBER, and CASPT2//B3LYP/AMBER calculations can be explained on the basis of the close CASPT2, B3LYP, and CASSCF equilibrium geometries for both W108• (left) and W48• (right) radicals (see Figure 5). In particular, the CASPT2 structures are very similar to the DFT structures, with deviations smaller than 0.01 Å. The major difference is found for the CASSCF structures relative to the N1−C2 bond, which is about 0.02 Å shorter than in the CASPT2 structures.

The excitation energies computed at the TDDFT/AMBER level, using the B3LYP and PBE0 functionals, give a blue-shift (0.11−0.22 eV) comparable to the CASPT2/AMBER calculations and a hypsochromic environmental shift of 10−15 nm (0.05−0.09 eV). Additional combinations of functionals and basis sets have been used to compute the vertical excitation energies, and the results are reported in Table S6.

Our computations also allowed for the characterization of the electronic structure of the spectroscopic excited state of W108• and W48•. In Figure 6 we report the CASSCF(11,10)/ANO-S-VDZP Mulliken spin population values that mainly contribute to the total spin population, for D_0 and the excited (D_2) state responsible for the observed electronic transition ($D_0 \rightarrow D_2$). The $D_0 \rightarrow D_1$ computed electronic transition (see Table S7) is weak compared to the $D_0 \rightarrow D_2$ one. Indeed, it has negligible oscillator strength and corresponds to an absorption in the IR region. The other electronic transition having non-negligible oscillator strength is the $D_0 \rightarrow D_4$, with an absorption maximum around 300 nm, which is consistent with the presence in that region of a peak in the experimental spectrum (see SI and ref 21). Interestingly, in both neutral radicals the transition is characterized by a displacement of the spin population toward the benzene ring that is holding the radical center in the D_2 excited state. This displacement is accompanied by a change in the charge distribution (see the Figure 6B) and a change,

dx.doi.org/10.1021/ja400464n | J. Am. Chem. Soc. 2013, 135, 4822−4833

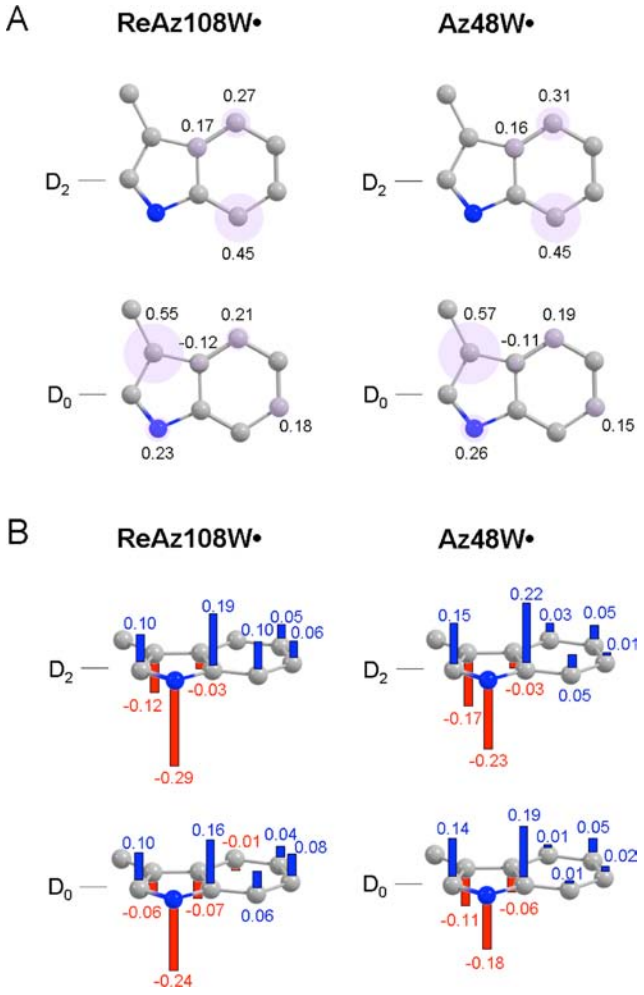

Figure 6. Mulliken spin population values (A) and charge distribution (B) of the D_0 and D_2 states for W108• (left) and W48• (right) computed at their CASPT2/AMBER D_0 equilibrium geometries. Fraction of positive (blue) and negative (red) charge is shown with colored bars along with the corresponding values (atomic charges with hydrogens summed into heavy atoms). The total Mulliken spin population is equal to 1, and the total Mulliken charge is equal to 0, adding the small contributions from the remaining QM atoms.

although limited, in dipole moments (see $\Delta\mu$ values in Table 3). In particular, *the D_2 excited state, for both W48• and W108•, features a more negative pyrrole moiety and a more positive benzene ring with respect to D_0*. Thus, upon excitation, the Trp• undergoes an increased charge separation that can be stabilized by a suitable polar environment. *This effect may justify the diverse responses of W108• and W48• to their different environments. Indeed, the D_2 excited state of the solvent-exposed W108• should be stabilized more than the D_2 of the W48• embedded in a hydrophobic environment*. This should result in a decreased D_0−D_2 energy gap for W108• and a corresponding red-shift of the absorption maximum in accord with experiments.

The good agreement between experimental and computed vertical excitation energies for ReAz108W• and Az48W• prompts for a detailed analysis of the factors determining the observed hypsochromic shift. In particular, it is important to establish if such shift is due to a change in chromophore (i.e., indole radical) geometry, field (e.g., electrostatic) effects due to the protein/solvent environment or to specific molecular interactions such as hydrogen bonding with residues or solvent molecules. Accordingly, in Figure 7, the CASPT2/ANO-S-

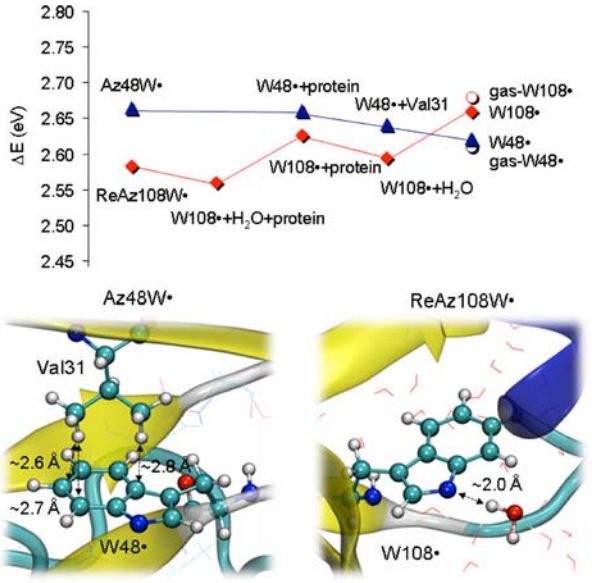

Figure 7. (Top) Analysis of the CASPT2//B3LYP/AMBER D_0→D_2 excitation energies of W108• (full rhombs) and W48• (full triangles). The D_0→D_2 energies of the chromophore inside the full protein (ReAz108W• and Az48W•) are compared to the excitation energies of (i) isolated chromophores taken with their protein-optimized geometries (W108• and W48•) and (ii) subsystems obtained by adding to W108• and W48• the effects of the protein residues or solvent molecules (each fragment is taken with the geometry optimized for the full protein). The same values for the isolated gas-phase optimized chromophores (gas-W108• and gas-W48•) are also shown (empty circles). (Bottom) Structure and major geometrical parameters for the relevant specific residue−chromophore interactions in Az48W• and ReAz108W•.

VDZP//B3LYP/6-31G**#/AMBER excitation energies for both systems are compared with those of (i) the isolated gas-phase optimized chromophores (gas-W108• and gas-W48•), (ii) the isolated chromophores (W108• and W48•) taken with their protein-optimized geometries, and (iii) a few subsystems obtained by adding to W108• and W48• the effects of the protein residues or solvent molecules.

The results show that the observed blue-shift in absorption going from ReAz108W• to Az48W• cannot be ascribed to a change in Trp• geometry. Indeed, W108• and W48• have excitation energies that are close to those of gas-W108• and gas-W48•. This is obviously due to a limited protein-induced change in the chromophore equilibrium geometries with respect to the gas phase. Such a conclusion is confirmed by the data in Figure S2, pointing to a <0.014 Å difference between the geometrical parameters of gas-W108• and gas-W48• compared to those of W108• and W48•. [We used two different reference structures for the gas-phase isolated chromophores because of the two different orientations of Trp in ReAz108W• and Az48W• (see the optimized structures in Figure S2).]

The analysis reported in Figure 7 also reveals that the excitation energy computed for Az48W• differs from that of W48• by +0.04 eV. The same difference is computed for a model where the solvent is removed from Az48W• (W48•+protein), thus demonstrating that the environmental

dx.doi.org/10.1021/ja400464n | J. Am. Chem. Soc. 2013, 135, 4822−4833

effect on the absorption of W48• is exclusively due to the protein residues. On the other hand, in ReAz108W•, a model lacking the solvent (W108•+protein) displays an opposite −0.05 eV shift with respect to W108• which is >50% of the difference in excitation energy between ReAz108W• and W108• (−0.08 eV). Thus, the interaction with the solvent significantly contributes to determine the shift in excitation energy of ReAz108W•. This is in accord with the expected red-shift in a polar environment on the basis of the nature of the $D_0 \rightarrow D_2$ electronic transition discussed before.

It is important to establish if the environmental effects are modulated by specific rather than field interactions. To this end we investigate the effect of the nearby Val31 side chain on the excitation energy of Az48W• (see Figure 7 bottom left). Indeed, we found that this residue causes a blue-shift of 0.02 eV, which accounts for ∼50% of the effect exerted by the whole protein residues (W48•+protein). The remaining cavity residues have, taken individually, a much smaller effect. The origin of the Val31 effect could be related to the proximity of the hydrogens of the CH_3 groups of Val31, carrying a partial positive charge, to the benzene ring which is carrying a positive charge as well. Thus, the computed increase in excitation energy could originate from this destabilizing interaction.

The results of a similar analysis for ReAz108W• allow us to conclude that the major effect exerted by the environment on the excitation energy is due to the presence of a specific H-bonded water molecule (linked to the N of the pyrrole moiety) (see Figure 7 bottom right). In fact, adding this water molecule to the isolated W108• leads to a red-shift of 0.07 eV, which derives from the H-bonded water dipole that stabilizes the negative charge on the pyrrole moiety. This effect is also evident from the computed shift on going from W108•+protein to W108•+H_2O+protein.

Remarkably, the excitation energies of W48•+protein and W108•+protein, i.e., considering the effect of the protein residue only, are computed to be similar, thus confirming again that *the effect of the different environment, i.e. polar (in ReAz108W•) vs apolar (in Az48W•), can be ascribed to the presence of the solvent in ReAz108W• and in particular to the presence of a specific H-bonded water molecule.*

3.3. Resonance Raman. The sub-picosecond time resolution of RR spectroscopy makes it possible to obtain structural information in real time on long-range ET reactions involving amino acid radical intermediates, which are not accessible to magnetic resonance and optical absorption experiments.

The computed vs observed RR difference spectra (514.5 nm excitation) of ReAz108W• and Az48W• are displayed in Figure 8 and clearly show that the protein environment exerts a strong influence on the vibrational frequencies and band intensities of Trp•.[21] The majority of peaks are downshifted in Az48W• relative to solvent-exposed ReAz108W•, with the exception of W7•, W16•, and W19• modes. On the basis of mode assignments and RR frequency differences between the radical and the closed-shell Trp species as well as between the buried and the solvent-exposed Trp•, Shafaat et al.[21,32] have identified modes that are most sensitive to solvent, protein environment,and/or hydrogen-bonding changes. These include W1•, W5•, W12•, W13•, and W17• modes. Interestingly, the calculated decrease in frequency for Az48W• is the largest for W1•, W12•, W13•, and W17• modes,with the frequency change ranging from −10 to −18 cm^{-1} (see Table S13). Therefore, our calculations are fully consistent with the experimentally

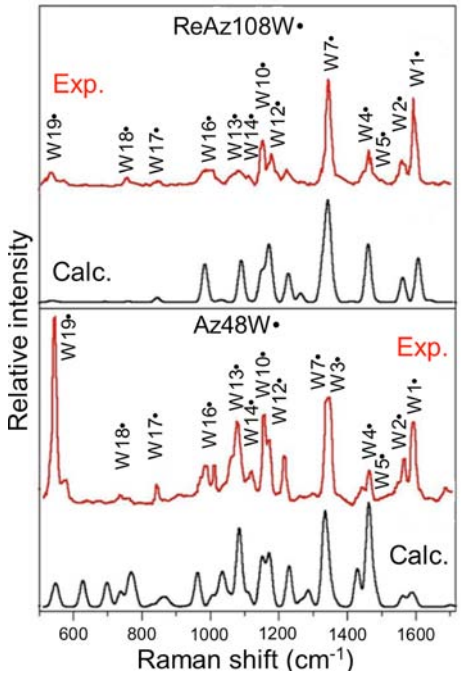

Figure 8. Experimental (red) and computed (black) RR spectra of ReAz108W• (top) and Az48W• (bottom). The experimental spectra are adapted from ref 21.

observed shifts of −8 to −13 cm^{-1} in the solvent-buried Trp•.[21] The intensity pattern is also sensitive to the environment with the largest differences occurring in the 1050−1250 cm^{-1} range and W12•, W10•, W14•, and W13• bands being more intense in Az48W•. This trend is captured by the simulations, but the intensity differences between two species do not become as pronounced as in the experiment (Figure 8).

The intense W1•, W5•, W12•, and W13• bands were predicted by Kim's group[21] to be dominated by ring breathing and stretching motions. We can support this assignment for W12• modes; however, for the W1•, W5•, and W13• modes the original assignment needs to be revised. In the light of our QM/MM-based results, the latter modes involve not solely ring breathing/stretching vibrations but also a significant movement of the β-methylene group in the protein backbone. A prominent C_β vibration can also be detected in the W3• mode. Substantial frequency shifts of the W1•, W5•, W12•, and W13• modes may be explained by a perturbed in-plane indole electron density in Az48W• relative to ReAz108W•.

The W17• mode involves a combination of a pyrrole ring vibration and a significant nitrogen movement. It downshifts by 18 cm^{-1} for Az48W•, in nice agreement with the experimental shift of 11 cm^{-1}, supporting the finding[32] that the W17• frequency increase is positively correlated with the strength of the N−H hydrogen bond. In fact, this mode may be considered as a good hydrogen bond indicator, and our results are compatible with Trp• H-bonded in ReAz108W• and not in Az48W•. Also, the W4• mode reveals prominent nitrogen displacement, resulting in an altered frequency of this mode being observed upon hydrogen bonding in ReAz108W•. B3LYP calculations predict a 4 cm^{-1} upshift on going from Az48W• to ReAz108W•, which is in excellent agreement with a 6 cm^{-1} upshift determined by the experimental studies. A band near 1130 cm^{-1} has been assigned to the W14• mode, which is

dx.doi.org/10.1021/ja400464n | J. Am. Chem. Soc. 2013, 135, 4822−4833

mainly due to a N−C2 stretch, and its −13 cm^{-1} shift was calculated for Az48W• compared to ReAz108W•. Experimental study reports this shift to be −3 cm^{-1}.

The most prominent difference in RR spectra of both radicals is a peak found at ∼540 cm^{-1} (W19•) which was assigned as in-plane benzene−pyrrole ring breathing coupled with the significant displacement of C_β in the protein backbone. This mode experimentally reveals a 7 cm^{-1} shift in Az48W• relative to ReAz10W•. We find our data in agreement with the proposed assignment, and additionally the calculated frequency shift perfectly matches the experimental value. This feature is very intense in Az48W• and rather weak in ReAz108W•. Although the theory does not perform particularly well to reproduce the absolute intensities of this mode in both species, the intensity ratio of this band in Az48W• and ReAz108W• (∼8) agrees nicely with the experiment.[21]

3.4. Excited-State Relaxation and Emission Maximum.

The analysis and interpretation of the vibronic structure described above allow us to conclude that, upon $D_0 \rightarrow D_2$ excitation, the Trp• radical relaxes along an in-plane stretching mode consistently with the observed RR spectrum. However this initial excited-state relaxation must lead to formation of a relaxed D_2 Trp•. In this section we predict the ReAz108W• and Az48W• D_2 equilibrium geometrical and electronic structures using multiconfigurational second-order perturbation theory (CASPT2).

In Figure 9 (top) we report the CASPT2/AMBER D_2 optimized equilibrium structures of ReAz108W• and Az48W•

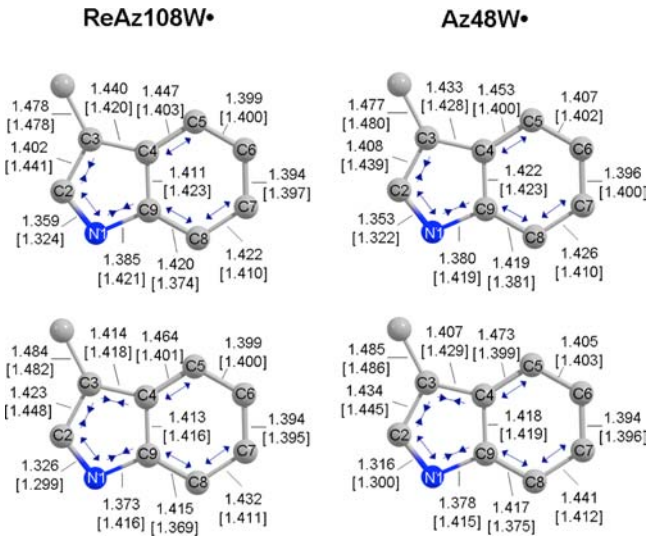

Figure 9. CASPT2/AMBER (top) and CASSCF/AMBER (bottom) D_2 versus D_0 (in square brackets) optimized geometries for W108• (left) and W48• (right). Bond length changes upon relaxation on D_2 excited state are represented by outward arrows (bond elongation) and inward arrows (bond contraction).

(the CASSCF/AMBER equilibrium structures are shown for comparison). Such D_2 structures are located ∼0.2 eV below the FC point. It is evident from the comparison of the D_0 and D_2 geometrical parameters that upon excitation Trp• must undergo a large geometrical deformation on the benzene moiety. In particular, the increasing length of both the C4−C5 and C9−C8 bonds leads to a butadienyl moiety which is only weakly interacting with the rest of the π-system. On the other hand the pyrrole moiety appears more symmetrical with the C2−C3 and C9−C4 bonds of closer length (∼1.40 and ∼1.41 in ReAz108W• and ∼1.41 and ∼1.42 Å in Az48W•, respectively). These changes in geometries are consistent with *an electronic structure where the radical center mainly resides on C8 or C5 of the butadienyl moiety and the pyrrole ring has now more closed-shell character* (see Figure 10A). Also, consistently,

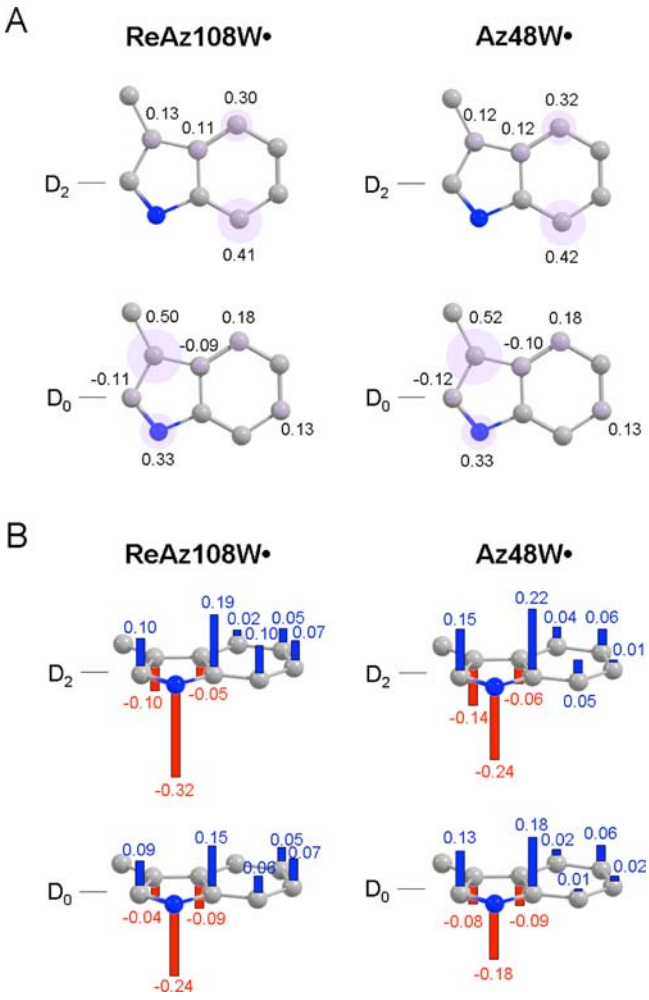

Figure 10. Mulliken spin population values (A) and charge distribution (B) of the D_0 and D_2 states for W108• (left) and W48• (right) computed at their CASPT2/AMBER D_2 equilibrium geometries. Fraction of positive (blue) and negative (red) charge is shown with colored bars along with the corresponding values (atomic charges with hydrogens summed into heavy atoms). The total Mulliken spin population is equal to 1, and the total Mulliken charge is equal to 0 adding the small contributions from the remaining QM atoms.

the D_2 state must have a different charge distribution where the benzene ring has a positive charge and the pyrrole moiety has a negative charge (see Figure 10B). In conclusion, the effect of the photoexcitation (see also Figure 6) and following relaxation is to move and stabilize the radical center from the pyrrole moiety to the benzene moiety which must become more electrophilic.

Using the above result and the data of Table 4 ,we predict a ∼560 and ∼540 nm emission for ReAz108W• and Az48W•, respectively. This emission has currently not been observed. The possibility of observing this emission is connected with the Trp• D_2 life expectation. This can be considerably shorter by barrierless access to surface crossings such as a D_2/D_1 and then

dx.doi.org/10.1021/ja400464n | J. Am. Chem. Soc. 2013, 135, 4822−4833

Table 4. CASPT2/AMBER and CASPT2//CASSCF/AMBER Emission Maxima λ_{max} (nm), Emission Energies (eV), Oscillator Strengths (f_{osc}), and Change in Dipole Moments ($\Delta\mu$) for ReAz108W$^\bullet$ and Az48W$^\bullet$

	ReAz108W$^\bullet$				Az48W$^\bullet$			
	λ_{max}	E	f_{osc}	$\Delta\mu$	λ_{max}	E	f_{osc}	$\Delta\mu$
CASPT2/ANO-S-VDZP//CASPT2(11,10)/6-31G**#								
CAS(11,10)[a]	560.6	2.21	0.0210	1.02	539.6	2.30	0.0159	1.86
CAS(11,10)[b]	602.3	2.06	0.0210	1.02	582.1	2.13	0.0159	1.86
CASPT2/ANO-S-VDZP//CASSCF(11,10)/6-31G**#								
CAS(11,10)[a]	544.8	2.28	0.0168	0.86	529.3	2.35	0.0119	1.84
CAS(11,10)[b]	587.2	2.11	0.0168	0.86	573.1	2.17	0.0119	1.84

[a]Computed using the standard IPEA Hamiltonian. [b]Computed without the IPEA shift.

D_1/D_0 conical intersections. Further work will be devoted to explore these issues.

4. CONCLUSIONS

In this work we used different QM/MM protocols to compute the EPR properties (hfcc's, **g**-tensors, and Mulliken spin densities), the vertical excitation and emission energies, and the UV−vis and RR spectra of solvent-exposed W108$^\bullet$ in ReAz108W$^\bullet$ and those of W48$^\bullet$ in the hydrophobic pocket of Az48W$^\bullet$. It is worthwhile to note that, within the employed QM/MM protocols, the optimized equilibrium structures of Trp$^\bullet$ have been obtained using, among other QM methods such as CASSCF and DFT, the *state-of-the-art* CASPT2 method.

The agreement between EPR, UV−vis, and RR experimental and computational data, along with the simulation of the observed hypsochromic shifts, indicates that our computer models provide a proper description of the real systems. Using these models we have been able to confirm, in accord with the experimental results of refs 21 and 22, the presence of a neutral Trp$^\bullet$ H-bonded in ReAz108W$^\bullet$ and not H-bonded in Az48W$^\bullet$. Indeed, the smaller value computed for the g_x component of the **g**-tensor for W108$^\bullet$ in ReAz108W$^\bullet$ compared to that of W48$^\bullet$ in Az48W$^\bullet$ represents unambiguous evidence in this direction. The computed increase in frequency for the W17$^\bullet$ mode in the RR spectrum of ReAz108W$^\bullet$, with respect to that of Az48W$^\bullet$, is a further proof of the involvement of a H-bonded Trp$^\bullet$ as intermediate in the ET reaction of ReAz108W$^\bullet$.

Another achievement of the present paper is the demonstration that the UV−vis spectra of ReAz108W$^\bullet$ and Az48W$^\bullet$ originate from a single electronic transition ($D_0 \rightarrow D_2$) and that the double-band line shape arise from a vibrational progression. We have also been able to characterize the electronic structure of the D_2 excited state of W108$^\bullet$ and W48$^\bullet$ and identify the effect exerted by a H-bonded water molecule in ReAz108W$^\bullet$ as the major contribution to the observed hypsochromic shift. In particular, the ReAz108W$^\bullet$ and Az48W$^\bullet$ models could be employed to disentangle the molecular-level interactions responsible for the shift. The results of this analysis reveal that, in ReAz108W$^\bullet$, the presence of hydrogen bonding between the W108$^\bullet$ and a single specific surface water molecule represents an effective means of spectral modulation. Similarly, the Az48W$^\bullet$ excitation energy is tuned by a specific electrostatic interaction between the radical moiety and residue Val31. These modulations appear to be mediated by the increase in nitrogen negative charge of the spectroscopic D_2 state with respect to the D_0 state of Trp$^\bullet$. Finally, we used the same ReAz108W$^\bullet$ and Az48W$^\bullet$ models to predict the relaxed Trp$^\bullet$ D_2 structures and corresponding emission maxima. To this end we found that the effect of the environment on the emission maxima must parallel that of D_0 absorption maxima.

We believe that the results presented here constitute an advancement of the understanding of the features that characterize the magnetic, electronic, and vibrational spectra of Trp$^\bullet$ and that cause the different environmental response. Furthermore, the knowledge acquired opens the way to the investigation of Trp-mediated electron- and H-atom-transfer reactions.

■ ASSOCIATED CONTENT

Ⓢ Supporting Information

QM/MM scheme; more computational details and tables; additional results on UV−vis properties of closed-shell Trp in ReAz108W and Az48W. This material is available free of charge via the Internet at http://pubs.acs.org.

■ AUTHOR INFORMATION

Corresponding Author

adalgisa.sinicropi@unisi.it

Notes

The authors declare no competing financial interest.

■ ACKNOWLEDGMENTS

We acknowledge the CINECA Awards No. HP10C9HMGL and No. HP10CJ65S2, 2011, for the availability of high-performance computing resources and support. This work was supported by the Italian MIUR PRIN 2009 project no. 2009STNWX3_001. M.O. is grateful to the National Science Foundation for grant nos. CHE-1152070 and to the Human Frontier Science Program Organization for grant RGP0049/2012CHE09-56776. T.A. acknowledges a statuary activity subsidy from the Polish Ministry of Science and Higher Education for the Faculty of Chemistry of Wroclaw University of Technology.

■ REFERENCES

(1) Stubbe, J.; Der Donk, W. A. *Chem. Rev.* **1998**, *98*, 705−762.
(2) Aubert, C.; Vos, M. H.; Mathis, P.; Eker, A. P. M.; Brettel, K. *Nature* **2000**, *405*, 586−590.
(3) Stubbe, J.; Nocera, D. G.; Yee, C. S.; Chang, M. C. Y. *Chem. Rev.* **2003**, *103*, 2167−2201.
(4) Kim, S. T.; Sacar, A.; Essenmacher, C.; Babcock, G. T. *Proc. Natl. Acad. Sci. U.S.A.* **1993**, *90*, 8023−8027.
(5) Aubert, C.; Mathis, P.; Eker, A. P.; Brettel, K. *Proc. Natl. Acad. Sci. U.S.A.* **1999**, *96*, 5423−5427.
(6) Sivaraja, M.; Goodin, D. B.; Smith, M.; Hoffman, B. M. *Science* **1989**, *245*, 738−740.
(7) Pelletier, H.; Kraut, J. *Science* **1992**, *258*, 1748−1755.

(8) Barrows, T. P.; Bhaskar, B.; Thomas, L. P. *Biochemistry* **2004**, *43*, 8826−8834.
(9) Lendzian, F.; Sahlin, M.; MacMillan, F.; Bittl, R.; Fiege, R.; Pötsch, S.; Sjöberg, B.-M.; Gräslund, A.; Lubitz, W.; Lassmann, G. *J. Am. Chem. Soc.* **1996**, *118*, 8111−8120.
(10) Sahlin, M.; Lassmann, G.; Pötsch, S.; Slaby, A.; Sjöberg, B. M.; Gräslund, A. *J. Biol. Chem.* **1994**, *269*, 11699−11702.
(11) Bleifuss, G.; Kolberg, M.; Pötsch, S.; Hofbauer, W.; Bittl, R.; Lubitz, W.; Gräslund, A.; Lassmann, G.; Lendzian, F. *Biochemistry* **2001**, *40*, 15362−15368.
(12) Blodig, W.; Smith, A. T.; Winterhalter, H. K.; Piontek, K. *Arch. Biochem. Biophys.* **1999**, *370*, 86−92.
(13) Pogni, R.; Baratto, M. C.; Giansanti, S.; Teutloff, C.; Verdin, J.; Valderram, B.; Lendzian, F.; Lubitz, W.; Vazquez-Duhalt, R.; Basosi, R. *Biochemistry* **2005**, *44*, 4267−4274.
(14) Pogni, R.; Baratto, M. C.; Teutloff, C.; Giansanti, S.; Ruiz-Duenas, F. J.; Choinowski, T.; Piontek, K.; Martinez, A. T.; Lendzian, F.; Basosi, R. *J. Biol. Chem.* **2006**, *28*, 9517−9526.
(15) Pogni, R.; Teutloff, C.; Lendzian, F.; Basosi, R. *Appl. Magn. Reson.* **2007**, *31*, 509−526.
(16) Pérez-Boada, M.; Ruiz-Dueñas, F. J.; Pogni, R.; Basosi, R.; Choinowski, T.; Martínez, M. J.; Piontek, K.; Martínez, A. T. *J. Mol. Biol.* **2005**, *354*, 385−402.
(17) Ruiz-Dueñas, F. J.; Pogni, R.; Morales, M.; Giansanti, S.; Mate, M. J.; Romero, A.; Martínez, M. J.; Basosi, R.; Martínez, A. T. *J. Biol. Chem.* **2009**, *284*, 7986−7994.
(18) Dempsey, J. L.; Winkler, J. R.; Gray, H. B. *Chem. Rev.* **2010**, *110*, 7024−7039.
(19) Warren, J. J.; Tronic, T. A.; Mayer, J. M. *Chem. Rev.* **2011**, *110*, 6961−7001.
(20) Jeschke, G. *Biochim. Biophys. Acta* **2005**, *1707*, 91−102.
(21) Shafaat, H. S.; Leigh, B. S.; Tauber, M. J.; Kim, J. E. *J. Am. Chem. Soc.* **2010**, *132*, 9030−9039.
(22) Stoll, S.; Shafaat, H. S.; Krzystek, J.; Ozarowski, A.; Tauber, M. J.; Kim, J. E.; Britt, R. D. *J. Am. Chem. Soc.* **2011**, *133*, 18098−18101.
(23) Walden, S. E.; Wheeler, R. A. *J. Phys. Chem.* **1996**, *100*, 1530−1535.
(24) Jensen, G. M.; Goodin, D. B.; Bunte, S. W. *J. Phys. Chem.* **1996**, *100*, 954−959.
(25) Himo, F.; Eriksson, L. A. *J. Phys. Chem. B* **1997**, *101*, 9811−9819.
(26) Svistunenko, D. A.; Adelusi, M.; Dawson, M.; Robinson, P.; Bernini, C.; Sinicropi, A.; Basosi, R. *Stud. UBB Chem.* **2011**, *56*, 135−146.
(27) Un, S. *Magn. Reson. Chem.* **2005**, *43*, S229−S236.
(28) Bernini, C.; Pogni, R.; Ruiz-Dueñas, F. J.; Martínez, A. T.; Basosi, R.; Sinicropi, A. *Phys. Chem. Chem. Phys.* **2011**, *13*, 5078−5098.
(29) Bernini, C.; Pogni, R.; Basosi, R.; Sinicropi, A. *Proteins: Struct., Funct. Bioinform.* **2012**, *80*, 1476−1483.
(30) Gurudas, U.; Schelvis, P. M. *J. Am. Chem. Soc.* **2004**, *126*, 12788−12789.
(31) Zieba, A. A.; Richardson, C.; Lucero, C.; Dieng, S. D.; Gindt, Y. M.; Schelvis, P. M. *J. Am. Chem. Soc.* **2011**, *133*, 7824−7836.
(32) Shafaat, H. S.; Leigh, B. S.; Tauber, M. J.; Kim, J. E. *J. Phys. Chem. B* **2009**, *113*, 382−388.
(33) Li, H.; Robertson, A. D.; Jensen, J. H. *Proteins* **2005**, *61*, 704−721.
(34) Humphrey, W.; Dalke, A.; Schulten, K. *J. Mol. Graphics* **1996**, *14.1*, 33−38.
(35) Jorgensen, W. L.; Chandrasekhar, J.; Madura, J. D.; Impey, R. W.; Klein, M. L. *J. Chem. Phys.* **1983**, *79*, 926−935.
(36) Cornell, W. D.; Cieplak, P.; Bayly, C. I.; Gould, I. R.; Merz, K. M.; Ferguson, D. M.; Spellmeyer, D. C. *J. Am. Chem. Soc.* **1995**, *117*, 5179−5197.
(37) Wang, J.; Cieplak, P.; Kollman, P. A. *J. Comput. Chem.* **2000**, *21*, 1049−1074.
(38) Ponder, J. W.; Case, D. A. *Adv. Protein Chem.* **2003**, *66*, 27−85.
(39) Qiu, D.; Dasgupta, S.; Kozlowski, P. M.; Goddard, W. A. I.; Spiro, T. G. *J. Am. Chem. Soc.* **1998**, *120*, 12791−12797.
(40) Rajapandian, V.; Hakkim, V.; Subramanian, V. *J. Phys. Chem. B* **2010**, *114*, 8474−8486.
(41) Frisch, M. J.; Trucks, G. W.; Schlegel, H. B.; Scuseria, G. E.; Robb, M. A.; Cheeseman, J. R.; Montgomery, J. A., Jr.; Vreven, T.; Kudin, K. N.; Burant, J. C.; Millam, J. M.; Iyengar, S. S.; Tomasi, J.; Barone, V.; Mennucci, B.; Cossi, M.; Scalmani, G.; Rega, N.; Petersson, G. A.; Nakatsuji, H.; Hada, M.; Ehara, M.; Toyota, K.; Fukuda, R.; Hasegawa, J.; Ishida, M.; Nakajima, T.; Honda, Y.; Kitao, O.; Nakai, H.; Klene, M.; Li, X.; Knox, J. E.; Hratchian, H. P.; Cross, J. B.; Bakken, V.; Adamo, C.; Jaramillo, J.; Gomperts, R.; Stratmann, R. E.; Yazyev, O.; Austin, A. J.; Cammi, R.; Pomelli, C.; Ochterski, J.; Ayala, P. Y.; Morokuma, K.; Voth, G. A.; Salvador, P.; Dannenberg, J. J.; Zakrzewski, V. G.; Dapprich, S.; Daniels, A. D.; Strain, M. C.; Farkas, O.; Malick, D. K.; Rabuck, A. D.; Raghavachari, K.; Foresman, J. B.; Ortiz, J. V.; Cui, Q.; Baboul, A. G.; Clifford, S.; Cioslowski, J.; Stefanov, B. B.; Liu, G.; Liashenko, A.; Piskorz, P.; Komaromi, I.; Martin, R. L.; Fox, D. J.; Keith, T.; Al-Laham, M. A.; Peng, C. Y.; Nanayakkara, A.; Challacombe, M.; Gill, P. M. W.; Johnson, B. G.; Chen, W.; Wong, M. W.; Gonzalez, C.; Pople, J. A. *Gaussian 03*, Revision B.04; Gaussian, Inc.: Wallingford, CT, 2004.
(42) Phillips, J. C.; Braun, R.; Wang, W.; Gumbart, J.; Tajkhorshid, E.; Villa, E.; Chipot, C.; Skeel, R. D.; Kale, L.; K., S. *J. Comput. Chem.* **2005**, *26*, 1781−1802.
(43) Darden, T.; York, D.; Pederson, L. *J. Chem. Phys.* **1993**, *98*, 10089−10092.
(44) Aquiliante, F.; De Vico, L.; Ferré, N.; Ghigo, G.; Malmqvist, P.-Å.; Neogrady, P.; Pedersen, T. B.; Pitonak, M.; Reiher, M.; Roos, B. O.; Serrano-Andrés, L.; Urban, M.; Veryazov, V.; Lindh, R. *J. Comput. Chem.* **2009**, *31*, 224−247.
(45) Ponder, J. W. *Tinker4.2*, software tools for molecular design; http://dasher.wustl.edu/tinker, 2004.
(46) Ferré, N.; Olivucci, M. *J. Am. Chem. Soc.* **2003**, *125*, 6868−6869.
(47) Ferré, N.; Olivucci, M. *J. Mol. Struct. (Theochem)* **2003**, *632*, 71−82.
(48) Andruniow, T.; Ferré, N.; Olivucci, M. *Proc. Natl. Acad. Sci. U.S.A.* **2004**, *101*, 17908−17913.
(49) Pistolesi, S.; Sinicropi, A.; Pogni, R.; Basosi, R.; Ferré, N.; Olivucci, M. *J. Phys. Chem. B* **2009**, *113*, 16082−16090.
(50) Sinicropi, A.; Andruniow, T.; Ferrè, N.; Basosi, R.; Olivucci, M. *J. Am. Chem. Soc.* **2005**, *127*, 11534−11535.
(51) Andersson, K.; Malmqvist, P.-Å.; Roos, B. O. *J. Chem. Phys.* **1992**, *96*, 1218−1226.
(52) Neese, F. An ab initio, density functional and semiempirical program package, Version 2.8; Bonn University: Germany, 2010.
(53) Becke, A. D. *J. Chem. Phys.* **1993**, *98*, 5648−5652.
(54) Lee, C.; Yang, W.; Parr, R. G. *Phys. Rev. B* **1988**, *37*, 785−789.
(55) Stephens, P. J.; Devlin, F. J.; Chabalowski, C. F.; Frisch, M. J. *J. Phys. Chem.* **1994**, *98*, 11623−11627.
(56) Adamo, C.; Barone, V. *J. Chem. Phys.* **1999**, *110*, 6158−6169.
(57) Barone, V., *Recent Advances in Density Functional Methods*, Part I; Chong, D.P., Ed.; World Scientific Publishing Co.: 1995; pp 287- 334.
(58) Barone, V.; Polimeno, A. *Phys. Chem. Chem. Phys.* **2006**, *8*, 4609−4629.
(59) Godbout, N.; Salahub, D. R.; Andzelm, J.; Wimmer, E. *Can. J. Chem.−Rev. Can. Chim.* **1992**, *70*, 560−571.
(60) Frisch, M. J.; Trucks, G. W.; Schlegel, H. B.; Scuseria, G. E.; Robb, M. A.; Cheeseman, J. R.; Scalmani, G.; Barone, V.; Mennucci, B.; Petersson, G. A.; Nakatsuji, H.; Caricato, M.; Li, X.; Hratchian, H. P.; Izmaylov, A. F.; Bloino, J.; Zheng, G.; Sonnenberg, J. L.; Hada, M.; Ehara, M.; Toyota, K.; Fukuda, R.; Hasegawa, J.; Ishida, M.; Nakajima, T.; Honda, Y.; Kitao, O.; Nakai, H.; Vreven, T.; J. A. Montgomery, J.; Peralta, J. E.; Ogliaro, F.; Bearpark, M.; Heyd, J. J.; Brothers, E.; Kudin, K. N.; Staroverov, V. N.; Keith, T.; Kobayashi, R.; Normand, J.; Raghavachari, K.; Rendell, A.; Burant, J. C.; Iyengar, S. S.; Tomasi, J.; Cossi, M.; Rega, N.; Millam, J. M.; Klene, M.; Knox, J. E.; Cross, J. B.; Bakken, V.; Adamo, C.; Jaramillo, J.; Gomperts, R.; Stratmann, R. E.; Yazyev, O.; Austin, A. J.; Cammi, R.; Pomelli, C.; Ochterski, J. W.; Martin, R. L.; Morokuma, K.; Zakrzewski, V. G.; Voth, G. A.; Salvador, P.; Dannenberg, J. J.; Dapprich, S.; Daniels, A. D.; Farkas, O.;

Foresman, J. B.; Ortiz, J. V.; Cioslowski, J.; Fox, D. J. *Gaussian 09*, Revision B.01; Gaussian, Inc.: Wallingford, CT, 2010.
(61) Petrenko, T.; Neese, F. *J. Chem. Phys.* **2007**, *127*, 164319.
(62) Andruniow, T.; Olivucci, M. *J. Chem. Theor. Comput.* **2009**, *5*, 3096−3104.
(63) Sinnecker, S.; Flores, M.; Lubitz, W. *Phys. Chem. Chem. Phys.* **2006**, *8*, 5659−5670.
(64) Martin, E.; Samoilova, R. I.; Narasimhulu, K. V.; Lin, T.-J.; O'Malley, P. J.; Wraight, C. A.; Dikanov, S. A. *J. Am. Chem. Soc.* **2011**, *133*, 5525−5537.
(65) Pauwels, E.; Declerck, R.; Verstraelen, T.; De Sterck, B.; Kay, C. W. M.; Van Speybroeck, V.; Waroquier, M. *J. Phys. Chem. B* **2010**, *114*, 16655−16665.
(66) Hart, R.; O'Malley, P. J. *Biochim. Biophys. Acta* **2010**, *1797*, 250−254.
(67) Sinnecker, S.; Neese, F. *J. Comput. Chem.* **2006**, *27*, 1463−1475.
(68) Moon, S.; Patchkovskii, S.; Salahub, D. R. *J. Mol. Structure: THEOCHEM* **2003**, *632*, 287−295.
(69) Joly, L.; Antoine, R.; Allouche, A.-R.; Dugourd, P. *J. Am. Chem. Soc.* **2008**, *130*, 13832−13833.
(70) Solar, S.; Getoff, N.; Surdhar, P. S.; Armstrong, D. A.; A., S. *J. Phys. Chem.* **1991**, *95*, 3639−3643.